CONF-8604213--2

LBL-21556

Lawrence Berkeley Laboratory
UNIVERSITY OF CALIFORNIA

Presented at the International Workhop on Physics and Engineering in Computerized Multidimensional Imaging and Processing, Irvine, CA, April 4, 1986; and to be published in Journal of the SPIE

RECENT DEVELOPMENTS IN POSITRON EMISSION TOMOGRAPHY (PET) INSTRUMENTATION

S.E. Derenzo and T.F. Budinger

April 1986

Donner Laboratory

Biology & Medicine Division

Prepared for the U.S. Department of Energy under Contract DE-AC03-76SF00098

DISCLAIMER

Recent developments in positron emission tomography (PET) instrumentation*

Stephen E. Derenzo and Thomas F. Budinger

Lawrence Berkeley Laboratory and Donner Laboratory, Mail Stop 55-121
University of California, Berkeley, California 94720

Abstract

This paper presents recent detector developments and perspectives for positron emission tomography (PET) instrumentation used for medical research, as well as the physical processes in positron annihilation, photon scattering and detection, tomograph design considerations, and the potentials for new advances in detectors.

*Presented at the International Workshop on Physics and Engineering in Computerized Multidimensional Imaging and Processing, Irvine, California, April 4, 1986. To be published in the Proceedings of Photo-Optical Instrumentation Engineers, 1986

This work was supported in part by the Director, Office of Energy Research, Office of Health and Environmental Research of the U.S. Department of Energy, under Contract No. DE-AC03-76SF00098, and in part by the National Institutes of Health, National Heart, Lung, and Blood Institute under grant No. P01 HL25840.

LBL--21556

DE87 000046

Introduction

Positron emission tomography (PET) serves a unique and important role in medical research because it permits the non-invasive, quantitative study of biological processes as they occur using minute quantities of tracer material. Table 1 illustrates how biological processes in different organs are studied using a variety of labeled compounds.

Table 1- Positron tracers and the processes they measure

Heart:	
ionic ^{82}Rb	myocardial perfusion
^{11}C palmitate	fatty acid transport, oxidation
^{11}C or ^{13}N amino acids	protein synthesis, tissue anabolism
Brain:	
ionic ^{82}Rb	blood brain barrier breakdown
^{18}F deoxyglucose	glucose transport, phosphorylation
^{122}I iodoamphetamines	blood flow
$^{15}O_2$	oxygen utilization
^{15}O water	blood flow
^{11}CO hemoglobin	blood volume

In the following sections, we review the physical processes involved in PET, the primary design considerations in PET instrumentation, recent detector developments, and potential areas for new development.

Physical Processes in PET

The ability of PET instrumentation to measure dynamically tracer concentrations is strongly influenced by the physical processes involved in positron emission (Figure 1), the detection of the annihilation photons, and the tomographic reconstruction, which we summarize below:

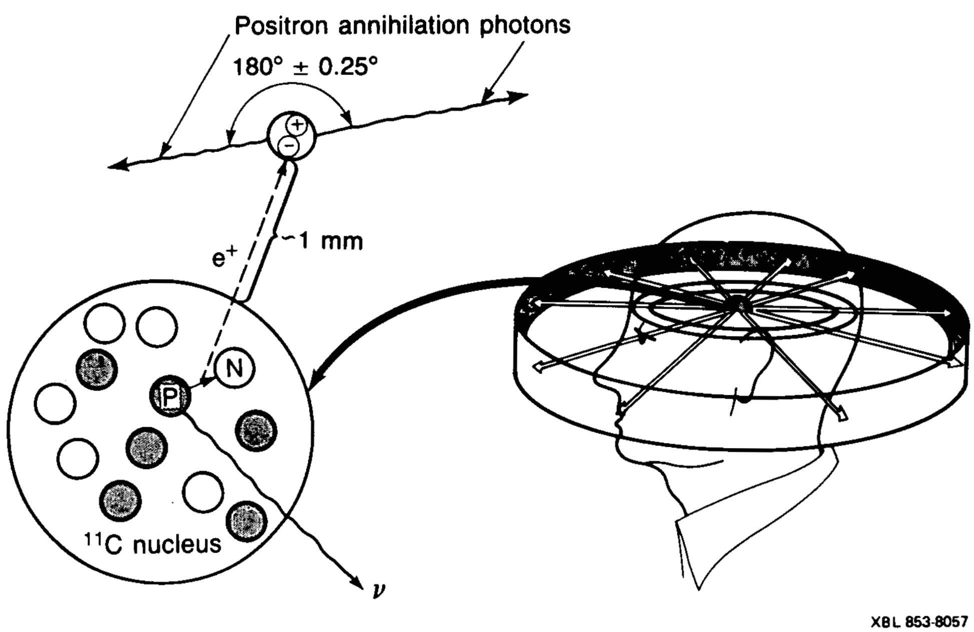

Figure 1: A positron emitted by nuclear decay stops in tissue and annihilates with a nearby electron, producing two 511 keV photons that fly off in nearly opposite directions.

(1) Positron emission: Positron emitting isotopes decay by transforming a proton in the nucleus into a neutron, a positron, and a neutrino.

(2) Positron stops in tissue: The positrons are emitted with a variety of energies, with a maximum energy that depends on the isotope. For example, ^{18}F, ^{11}C, ^{68}Ga, and ^{82}Rb have maximum positron energies of 0.64 MeV, 0.96 MeV, 1.90 MeV, and 3.35 MeV, respectively. The resulting positron range varies from a small fraction of a mm for ^{18}F to several mm for ^{82}Rb.[1–4]

(3) Positron-electron annihilation: The positron annihilates with an electron to produce two 511 keV photons. If the positron were able to loose all of its kinetic energy before annihilation, the two 511 keV annihilation photons would be emitted in exactly opposite directions. However, the positron has a residual energy of typically 10 eV at annihilation, and the emission angle has a Gaussian distribution with a full-width at half-maximum (fwhm) of 0.50°.[5]

(4) Scatter in tissue: A 511 keV photon will travel an average of 10 cm in water before interacting by Compton scattering. This process reduces its energy and randomly changes its direction, effectively losing all image information. The human head or chest is approximately two interaction lengths thick, and the probability that both annihilation photons leave the body unscattered is only about 20%.[6] This represents a significant loss of events and requires large correction factors. Also, a small but significant fraction of the annihilation photons scatter "in the plane" of the tomograph and are detected as prompt (non-random) coincidences. These result in a heterogeneous background that extends beyond the subject over the entire imaging field.

(5) Interaction with the detectors: The annihilation photons that reach the scintillators can interact in two ways– (i) by photoelectric effect, whereby the entire 511 keV is given to a recoil electron, or (ii) by Compton scattering, where only a portion of the photon energy is given to a recoil electron and the photon is reduced in energy and scattered into a new (random) angle. For BGO the probability of a photoelectric event is about 50% for the first interaction. For BaF_2 this probability is about 25%. A successful event requires that both annihilation photons pass the pulse height requirements in the opposing detectors.[7,8] The *detection efficiency* is the fraction of annihilation photons reaching the scintillator that produce an acceptable pulse.

(6) Scintillation: The recoil electrons produce ionization and excited atomic electrons in the scintillation crystal. Some of the excited electrons return to their ground states by the emission of scintillation light. The *luminous efficiency* (number of scintillation photons per keV loss) and the speed of emission vary from crystal to crystal.[9]

(7) Light Transfer to Photodetector: Light in the scintillator can be trapped by total internal reflection, scattered or absorbed by internal impurities and imperfections, scattered or absorbed by external reflectors, or collected by the photodetector. The *light collection efficiency* is the fraction of light that reaches the photodetector.[10]

(8) Production of an electrical pulse: The photodetector converts collected scintillation light to a useful electrical pulse. The *quantum efficiency* is the probability that an incident photon will produce a photoelectron in the photodetector. The photomultiplier tube has an internal gain of typically 1 million and a single photoelectron produces a pulse several nsec wide and many mV high.

(9) Electronics: Electronic circuits determine whenever two opposing crystals have detected photons within a short time interval (5 to 20 nsec, depending on the detector material) and store the addresses of the crystals involved.[11,12] For the time-of-flight mode, the differential time of arrival is also recorded.[13,14]

(10) Attenuation correction: Before the administration of any radioactive isotope, the patient or animal is placed in the tomograph and positioned at the slice to be imaged. An external positron source (usually 275-day ^{68}Ge) encircles the patient, and the tomograph measures the annihilation photons that pass through the patient unscattered. These measurements are used to correct the emission data for attenuation through the patient.

(11) Additional data corrections: Before tomographic reconstruction, the data must also be corrected for (i) accidental background events (random coincident detections of unrelated annihilation photons), (ii) scattered background events (coincident detections of photon pairs from the same positron but one or both have scattered), and (iii) the loss of events due to deadtime in the detectors and electronics.

(12) Reconstruction: The tomographic reconstruction usually involves filtering the parallel-ray projections either by convolution or frequency filtering and then back-projecting to form the image array. Alternate procedures involve iterative methods of estimating the true distribution such as maximum likelihood or least squares techniques.[15]

Note that 4 different efficiencies appear above: detection efficiency, luminous efficiency, light collection efficiency, and quantum efficiency.

Tomograph design factors

The goal of most tomograph designs is the accurate and rapid measurement of tracer concentration in sharply-defined tissue volume elements.[16–19] This requires temporal resolution, spatial resolution, and the quantitative measurement of activity concentration, as discussed below:

Quantitative accuracy–statistical factors

Statistical accuracy in the reconstructed image depends on the number of coincident events that can be collected within the available time. This is determined both by the available positron activity and the sensitivity of the tomograph, which is usually expressed as the number of coincident events detected per sec per μCi/cm^3 in a 20 cm diam cylinder of water. In addition, some detector materials provide time-of-flight information, which reduces statistical fluctuations in the reconstructed image. The system sensitivity depends on the following factors:

(1) Solid angle coverage: Multiple rings of detectors that encircle the patient provide the best acceptance solid angle for the annihilation photons. Utilization of the cross-ring coincidences is very important in realizing the full available solid angle.

(2) **Axial coverage:** Multiple detector rings also serve to cover a larger volume of tissue, thus providing a higher event rate for a given amount of administered tracer activity.

(3) **Detector Material:** (Table 2) Except for applications requiring very high light output, BGO has replaced NaI(Tl) in non-time-of-flight PET instrumentation. BGO has the highest density and the highest atomic number of any detector material, and as a result is best able to totally absorb 511 keV photons efficiently in small crystals. BaF_2 has replaced CsF for time-of-flight positron instrumentation. In 1982 a very fast (800 psec) scintillation component was discovered, making BaF_2 the highest speed inorganic scintillator known.[20] BaF_2 is not hygroscopic (unlike CsF) and the crystals do not have to be sealed in bulky cans, which improves the detection efficiency. For any detector material, the detection efficiency depends on the detector material, size, and pulse height thresholds used.[7,8]

Table 2. Detector materials for PET

Material	NaI(Tl)	CsF	BGO[a]	GSO[b]	BaF_2
Density (gm/cm^3)	3.67	4.61	7.13	6.71	4.8
Atomic Numbers	11,53	55,9	83,32,8	64,16,8	56,9
Emission wavelength (nm)	410	390	480	430	310;225
Index of refraction	1.85	1.48	2.15	1.9	1.56
Hygroscopic	YES	VERY	NO	NO	NO
Photoelectrons per 511 keV	3,000	200	400	600	800;200
Scintillation decay time (nsec)	230	2.5	300	60	620;0.8
Photoelectrons/ns (peak rate)	13	60	1.3	11	1.3;250

[a]bismuth germanate, $Bi_4Ge_3O_{12}$
[b]gadolinium orthosilicate (Cerium activated), $Gd_2SiO_5(Ce)$

(4) **Single vs multiple crystal detections:** Multicrystal detector designs fall into two categories. Those in the first category measure the amount of energy deposited in each crystal and can reject multiple crystal interactions to preserve the full spatial resolution of the detector crystals. Those in the second category estimate the center of energy deposition without determining how many crystals are involved. The multiple crystal events thus included appear to enhance the detection efficiency, but they also degrade the position resolution.

(5) **Time-of-flight information:** Modern BaF_2 detectors have excellent timing resolution (typically 400 psec fwhm) and are able to measure the arrival time difference between the two photons and determine the annihilation point with an

uncertainty of 6 cm fwhm. In conventional tomography, the annihilation point is only known to lie somewhere along the line between the two coincident detectors. The time-of-flight information is able to reduce the rms statistical uncertainty in the reconstructed image by the ratio of the distance across the emitting region to the time-of-flight uncertainty times twice the speed of light (15 cm per nsec).[21–28] For example, for a time-of-flight uncertainty of 6 cm and a 24 cm diam emission region, the time-of-flight information reduces the statistical uncertainty by a factor of 2 which corresponds to a four-fold decrease in the imaging time.[29,30] The detection efficiency ϵ and the timing resolution τ can be combined in the figure of merit ϵ^2/τ where ϵ^2 is proportional to the number of events detected and $1/\tau$ is proportional to the statistical value of each event.[8]

Quantitative Accuracy–systematic factors

PET data are subject to the following systematic errors:

1) Attenuation of the annihilation photons in the tissue[31,32]

2) Partial volume effects due to limited axial resolution[33]

3) In-plane smearing due to limited in-plane resolution[34]

4) Background events due to accidental coincidences (unrelated annihilation photons detected in coincidence by chance)[35–38] and prompt scattered events (annihilation pairs from the same positron where one or both have scattered).[37,39–42]

5) Deadtime losses in the detectors and electronic circuits.[43,44]

Temporal resolution

The ability to measure the tracer concentration with good temporal resolution (i.e. in a series of rapid time sequence images) requires the collection of a large number of events during the study, which requires good detection efficiency, low deadtime, high maximum data rates, and a minimum of detector motion. Note the ability to fit compartment model rate constants to PET data depends primarily on the total number of events collected in the study and the temporal resolution. The number of events in each time sequence image is of lesser importance.

Spatial resolution factors

Quantitation within regions of size D requires an overall system spatial resolution with fwhm $\leq$ D/2. Principal components of the system resolution are discussed below:

(1) Positron range: Accurate measurements of the positron annihilation distributions show a distribution with a bright center and extensive tails.[1-3] The resulting full-width at half-maxima are very small (< 1 mm) and 90% of the annihilations lie beyond this distance. For a summary of these results, and a method for mathematically removing this blurring factor, see ref 4.

(2) Deviations from 180° emission: Measurements of the angular distribution of annihilation photons in water at 20° show a nearly Gaussian distribution with a fwhm of $\Delta = 8.7$ mrad (0.50°).[5] The corresponding spatial distribution fwhm Γ at the center of a detector ring of diameter D is given by $\Gamma = (\Delta/4)(D) = 0.0022D$ This blurring factor is not easily removed mathematically and represents the most fundamental limit to spatial resolution in PET.

(3) Detector aperture: For discrete crystals of exposed width W, the geometrical component of the detector resolution (at the center of the imaging port) is approximately equal to W/2.[45-47]

(4) Linear sampling: For detectors of width W, the geometrical resolution of W/2 discussed in part (3) above will not be realized in the reconstructed image unless the tomographic sampling distance is W/4 or finer throughout the image region. A stationary circular array has a sampling distance of W/2. The most frequently employed method of improving the sampling is by the "wobble" motion–rotating the detector array about a small circle centered at the system axis[48-53] Other sampling schemes include irregularly spaced crystals[54,55] and selective rotation of crystal groups around the tomograph axis.[56] A sampling distance of W/4 can also be achieved with only two mechanical positions by using the "clam" motion [57]

(5) Multiple crystal interactions: Compton scattering of the annihilation photons in the detectors can result in a mis-identification of the detector of first interaction. This can be reduced by (i) coupling each scintillator to its individual photodetector and requiring single detector interactions only[58] or (ii) placing shielding material between the detectors, but this reduces the detection efficiency, especially for off-angle rays.[7,46,47]

(6) Off-axis penetration: Annihilation photons from off-axis sources can penetrate one or more detectors before interacting and the uncertainty of the depth of interaction results in a radial elongation of the PSF at the edge of the field.[59-61] Wedge-shaped crystals appear to have little benefit when the crystals are narrower than about 8 *mm*.[62]

(7) Reconstruction filter: For the best estimation of the tracer activity within regions of interest, the reconstruction filter upper frequency roll-off should be determined by the system resolution, not by statistical fluctuations.

(8) Organ motion: The effects of organ and tracer motion are reduced by gating for cardiac imaging and rapid sequence imaging for fast dynamic studies.

Recent detector developments

Small PMTs

The development of smaller photomultiplier tubes (PMTs) (especially the 14 mm and 10 mm diameter types) have permitted the construction of positron tomographs with 3 mm crystals,[63] 4 mm crystals,[64,65] and 5.6 mm crystals[66–68] where each crystal is coupled to one PMT.

Light division coding

In this class of detector design, each PMT is coupled to 2 or more crystals and the ratio (or difference) of the PMT signals is used to determine the crystal of interaction. This includes the MGH positron camera[69] built in the late 1960's, as well as the "analog coding" tomograph developed and built by the same group.[70–74] This is an area of active current interest, and numerous variations have been proposed and tested.[55,75–78]

Anger-type coding

In this scheme, a single large scintillation crystal is coupled to many PMTs and the ratio of outputs is used to determine the center of intensity. This design is basic to the Anger Scintillation Camera[79] and has been adapted for PET in the form of a hexagonal array of NaI(Tl) bars[80–82] for single slice imaging and in the form of larger crystals for multi-slice imaging.[83]

Wire chambers:

Considerable advances have been made over the years in the development of wire chamber-converter combinations for PET.[84–86] However, the detection efficiency and timing resolution are significantly poorer than the more conventional (although possibly more costly) scintillator-PMT approach.

A more recent development uses an efficient scintillation detector such as BaF_2 to produce UV emissions and a wire proportional chamber with a special liquid photocathode that can convert the UV into an electron avalanche.[87,88]

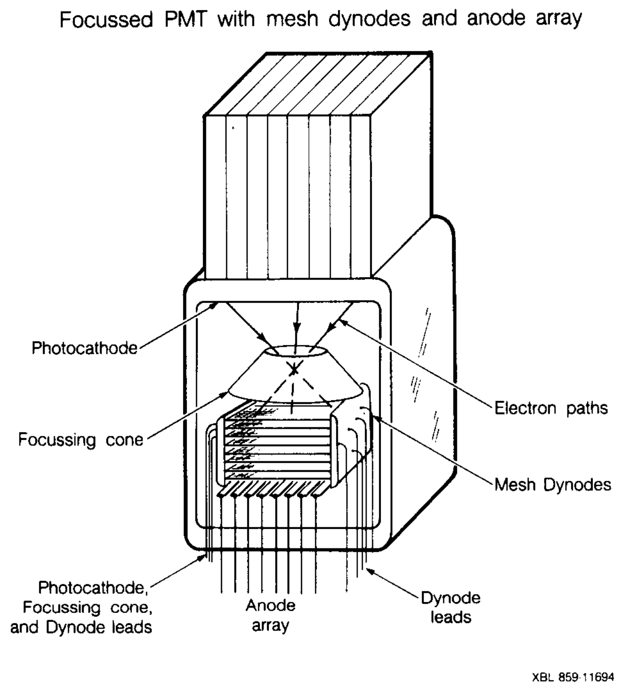

Figure 2: Design for a multi-anode PMT incorporating electron focussing and mesh dynodes

Position-sensing PMTs:

The μchannel PMT has been under development for several years[89–91] and has very high speed, but is limited by low packing density, high price, and relatively short useful lifetime.

A special PMT with two 12 mm x 24 mm phototubes in a single glass envelope was developed by Hamamatsu Corp. for a positron tomograph built by the National Radiological Institute of Japan.[92]

Recently, Hamamatsu Corp. has developed a mesh-dynode PMT that has a position sensing anode.[93–95] A recognized limitation of this approach is the dead space taken up by the support structures for the mesh dynodes and the anode. In order to couple this PMT to a close-packed crystal array, the workers at Hamamatsu have suggested a special lightpipe that matches the area of the crystals and tapers to a smaller area at the PMT window.

Figure 2 shows our suggestion for another solution to this packing problem, where a focussing cone is used to demagnifying the photocathode onto the first mesh dynode. The photocathode would be as large as the crystal array and the photoelectrons efficiently transported to the smaller first mesh dynode without losing position information. A tapered lightpipe would be less efficient.

Time-of-Flight

See references (21-28) for descriptions of positron tomographs using time-of-flight information for improved randoms rejection, high maximum data rates, and reduced statistical noise.

Avalanche Photodiode- BGO detectors

One approach for the eventual elimination of the glass PMT is the use of "solid state PMTs" in which electrons are multiplied in high field regions within the photodiode material.[96–101] At the present time, these devices are considerably more expensive than glass PMTs and have poorer timing resolution.

Lightpipes and external PMTS

For several years, an ambitious and novel high resolution positron tomograph design using plastic scintillators and a coded optical fiber readout has been investigated at Texas A&M University. A full tomograph would have 8 detector layers each consisting of 16 concentric rings of 1024 scintillators per ring (a total of 131,072 independent scintillators), and 356,352 optical fibers would couple the scintillators to 576 PMTs.[102]

Combined Phototube- solid state readout

This approach combines the excellent timing resolution of the PMT with the small size of solid state photodetectors (Figure 3). A group of crystals is coupled to a relatively large photomultiplier tube which determines the timing for the group. The solid-state photodetectors are coupled individually to each crystal to determine the identity of the scintillating crystal. Candidates for the photodetector include HgI_2,[103–106] silicon photodiodes,[45,107–109] GaAs photodiodes,[110] silicon avalanche photodiodes,[97–100] and small low-gain PMTs.[93] This method is good for very small crystals, since the noise of solid state photodetectors decreases with decreasing area, and the signal is nearly independent of crystal size. In addition, it permits the rejection of multiple-crystal interactions that degrade spatial resolution.

The feasibility of this concept has been demonstrated using a 3 mm wide BGO crystal in coincidence with two 3 mm wide BGO crystals coupled to a common 14 mm PMT and individually coupled to low-noise silicon photodiodes. The signal to noise ratio was adequate for the identification of the individual crystals on an event-by-event basis and the measured detector pair resolution was 2.0 mm fwhm.[45,108]

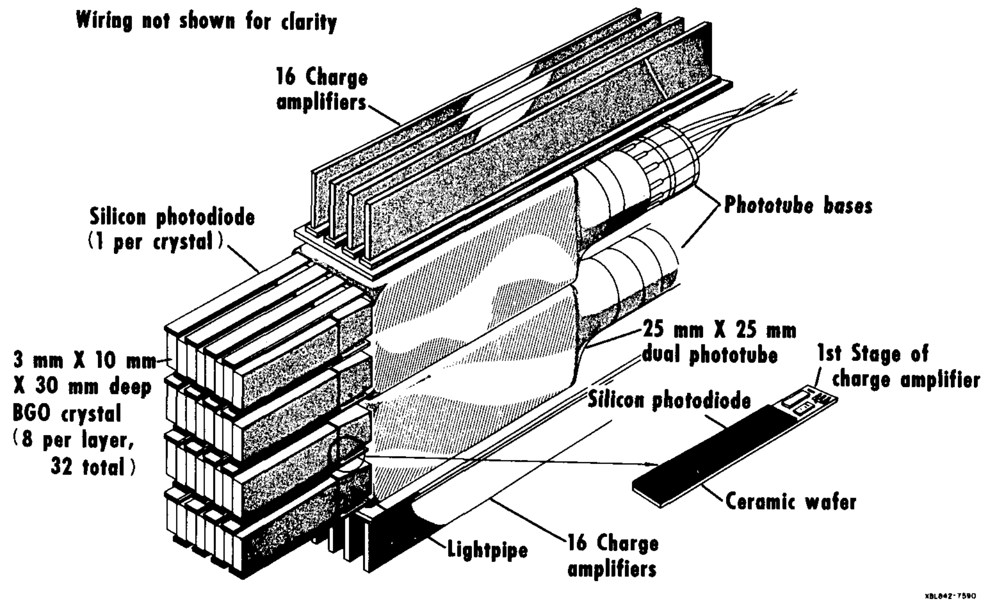

Figure 3: Schematic of 32 BGO crystals, 4 phototubes in 2 glass envelopes, 32 silicon photodiodes, and charge amplifiers. The phototubes provide group timing information and the silicon photodiodes and charge amplifiers determine (i) whenever an annihilation photon interacts in more than one crystal, (ii) the crystal of interaction, and (iii) the depth of interaction in the crystal. This approach provides the best possible spatial resolution for a given crystal array.

Figure 4: Low-noise position-sensitive silicon photodiode for the determination of energy deposited in the crystal and the depth of interaction.

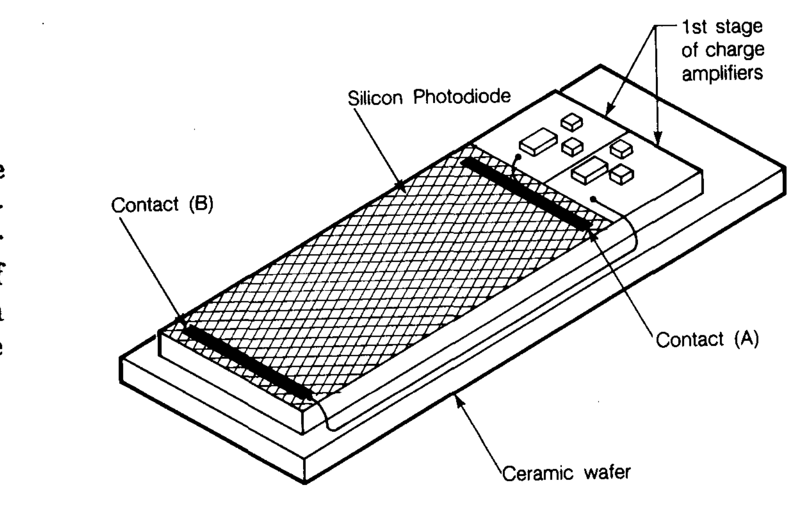

Moreover, by using position-sensitive solid-state photodetectors to measure the depth of interaction in the crystal, off-axis penetration effects can be nearly eliminated (Figure 4).

Scintillators with different decay times

By coupling scintillation crystals with significantly different light decay times such as BGO (300 nsec) and GSO (60 nsec),[111] or CsF (2.5 nsec) and BaF_2 (80% at 620 nsec and 20% at 0.8 nsec),[26] it is possible to determine the crystal of interaction by an analysis of the PMT pulse shape. However, multiple crystal interactions cause the slower detector to be chosen, even if both are involved.

To provide depth of interaction information as well as finer linear sampling, it has been recently proposed to use concentric rings of scintillation crystals having different light decay time.[112]

Advanced tomographs

Table 3 describes some advanced positron tomographs with an image resolution finer than 7 mm.

Table 3. Comparison[a] of positron tomographs with spatial resolutions finer than 7 mm fwhm

Institution	MGH Boston	NIRS Japan	CTI Knoxville	LBL Berkeley	Univ Penn
References	71-74	65,64	66	63	81,82
Detector Material	BGO	BGO	BGO	BGO	NaI(Tl)
Number of Rings	1	1	1-4	1	1
Number of Crystals	360	128	512[b]	600	6
Detector Ring Diam (cm)	46	26.5	100	60	85[c]
Patient Port Diam (cm)	28	13.5	65	30	50
Crystal Width (mm)	4	4	5.6	3	–
Crystal C-C Spacing (mm)	4.0	6.5	6.1	3.15	–
In-plane Resolution (mm)[d]	4.8	3	5	2.6[e]	6.5
Axial Resolution (mm)	10	5	18	5	13

[a] Count rate capabilities are not available and cannot be compared.
[b]per ring
[c]hexagonal
[d]FWHM of reconstructed point spread function near center of system
[e]A resolution of 2.4 mm is expected for the complete system.

Table 4 lists the three major contributions to spatial resolution at the center of a 60 cm diameter detector ring comprised of 3 mm wide BGO crystals, assuming that multiple crystal interactions are rejected. For positron emitters of low emission energy such as ^{18}F, the contributions from detector size (1.5 mm fwhm) and angulation error (1.3 mm fwhm) are the primary factors. This analysis is in excellent agreement with the measurements of References 45 and 63. In reference 63, the measured point spread function (PSF) had 2.6 mm fwhm at the center of the ring and crystal penetration increased the radial component of the PSF to 4.2 mm fwhm at a distance of 8 cm from the center.

Table 4. Contributions to spatial resolution using 3 mm wide BGO crystals

Detector size	1.5 mm (triangular)
Angulation error	1.3 mm (Gaussian)
Positron Range (^{18}F)	0.5 mm[a] (sharply peaked)
Combined detector pair resolution	2.0 mm[b]
Image resolution at system center	2.6 mm[c]

[a]calculated as 2.35 times the measured rms deviation
[b]above 3 contributions added in quadrature and in agreement with the measurements of Ref. 45
[c]25% increase due to reconstruction filter and in agreement with the measurements of Ref. 63

Areas for future development

Design factors

In future tomograph designs, the detector resolution will be improved to the point where (1) positron range, (2) deviations from 180° emission, (3) multiple crystal interactions, and (4) off-axis penetration become increasingly important.

The peaked nature of the positron range blurring function permits its mathematical removal. This reduces the systematic error due to blurring from one region to another and improves the estimation of the activity in each region.[4] The supression of positron range blurring by strong magnetic fields appears difficult, as fields higher than 5 Tesla would be required.[113]

It would also appear possible to remove the smearing effects of multiple-crystal interactions and off-axis crystal penetration by mathematical processing of the projection data before reconstruction. However, it is statistically preferable to eliminate these factors on an event-by-event basis by using detector designs that can reject multiple-crystal interactions and measure the depth of interaction in the detector.

The potential for new scintillators

Table 1 lists properties of the scintillation crystals most commonly used in positron tomographs. Of these, NaI(Tl) has the best photon yield and pulse height resolution, BaF_2 has the best timing resolution, and BGO has the best detection efficiency. An "ideal detector" with the best properties of all three has not yet been found. However, the scintillation properties of three of these crystals have been discovered rather recently: BaF_2 in 1971,[114] BGO in 1973,[115] the fast component of BaF_2 in 1982,[20,116] and GSO in 1982[117]. Further efforts in this direction are essential if the potentials of PET are to be fully realized.

The ultimate scintillator for PET would have the high atomic number and density of BGO, the high light output of NaI(Tl), and the ultra-fast decay of BaF_2 to combine high detection efficiency, good spatial resolution, high data rates, and the increased sensitivity provided by time-of-flight information.

Acknowledgements

I Thank R. Huesman and T. Budinger for helpful discussions.

This work was supported in part by the Director, Office of Energy Research, Office of Health and Environmental Research of the U.S. Department of Energy, under Contract No. DE-AC03-76SF00098, and in part by the National Institutes of Health, National Heart, Lung, and Blood Institute under grant No. P01 HL25840.

References

1. Phelps ME, Hoffman EJ, Huang SC, et al: Effect of positron range on spatial resolution. *J Nucl Med* **16:** 649-652, 1975

2. Cho ZH, Chan JK, Eriksson L, et al: Positron ranges obtained from biomedically important positron-emitting radionuclides. *J Nucl Med* **16:** 1174-1176, 1975

3. Derenzo, SE: Precision measurement of annihilation point spread distributions for medically important positron emitters. In: *Positron Annihilation,* Hasiguti

RR and Fujiwara K, eds, pp 819-823, The Japan Institute of Metals, Sendai, Japan, 1979

4. Derenzo SE: Mathematical removal of positron range blurring in high resolution tomography. *Trans Nucl Sci* **NS-33:** 565-569, 1986

5. Colombino P, Fiscella B, Trossi L: Study of positronium in water and ice from 22 to -144 °C by annihilation quantum measurements. *Nuovo Cimento* **38:** 707-723, 1965

6. Budinger TF, Derenzo SE, Gullberg GT, Greenberg WL, and Huesman RH: Emission computer assisted tomography with single-photon and positron annihilation photon emitter. *J Comput Assist Tomogr* **1:** 131-145, 1977

7. Derenzo SE: Monte Carlo calculations of the detection efficiency of arrays of NaI(Tl), BGO, CsF, Ge, and plastic detectors for 511 keV photons. *IEEE Trans Nucl Sci* **NS-28:** 131-136, 1981

8. Derenzo SE: Comparison of detector materials for time-of-flight positron tomography. *Proceedings of the International Workshop on Time-of-Flight Positron Tomography,* Thomas LJ and Ter-Pogossian MM, eds. pp 63-68, IEEE Computer Society Cat No 82CH1791-3, 1982

9. Birks JB: *The Theory and Practice of Scintillation Counting* Pergamon Press, Oxford, England, 1964

10. Derenzo SE and Riles J: Monte Carlo calculations of the optical coupling between bismuth germanate crystals and photomultiplier tubes. *IEEE Trans Nucl Sci* **NS-29:** 191-195, 1982

11. Huesman RH and Cahoon JL: Data acquisition, reconstruction and display for the Donner 280-crystal positron tomograph. *IEEE Trans Nucl Sci* **NS-27:** 474-478, 1980

12. Cahoon JL, Huesman RH, Derenzo SE, et al: The electronics for the Donner, high resolution 600-crystal positron tomograph. *IEEE Trans Nucl Sci* **NS-33:** 570-574, 1986

13. Blaine J, Ficke D, Hitchens R, et al: Data acquisition aspects of super-PETT. *IEEE Trans Nucl Sci* **NS-29:** 544-547, 1982

14. Philippe EA, Mullani N, Hartz E, et al: Real-time multi-processor image reconstructor for time-of-flight positron emission tomography (TOFPET). *IEEE Trans Nucl Sci* **NS-29:** 524-527, 1982

15. Huesman RH, Gullberg GT, Greenberg WL and Budinger TF: *Users Manual: Donner Algorithms for Reconstruction Tomography.* Lawrence Berkeley Laboratory, Publication PUB-214, 1977

16. Budinger TF and Huesman RH: Ten precepts for quantitative data acquisition and analysis. *Circulation* **72 Suppl. IV**-53, 1985

17. Budinger TF, Huesman RH, Knittel B, Friedland R, and Derenzo SE: Physiological modeling of dynamic measurements of metabolism using positron emission tomography. In *The Metabolism of the Human Brain Studied with Positron Emission Tomography,* T. Greitz and D. Ingvar, Eds, Raven Press, New York, pp 165-183, 1985

18. Huesman RH: A new fast algorithm for the evaluation of regions of interest and statistical uncertainty in computed tomography. *Phys Med Biol* **29:** 543-552, 1984

19. Mazoyer BM, Huesman RH, Budinger TF, Knittel BL: Dynamic PET data analysis: evaluation of the data acquisition protocol. *J Comp Assis Tomog* (in press) 1986

20. Gariod R, Allemand R, Cormoreche E, et al: The "LETI" positron tomograph architecture and time of flight improvements. *Workshop on Time-of-Flight Tomography,* IEEE Catalog No 82CH1719-3, 1982.

21. Allemand R, Gresset C, and Vacher J: Potential advantages of a Cesium Fluoride scintillator for a time-of-flight positron camera. *J Nucl Med* **21:** 153-155, 1980

22. Snyder DL, Thomas LJ and Ter-Pogossian MM: A mathematical model for positron-emission tomography systems having time-of-flight measurements. *IEEE Trans Nucl Sci* **NS-28:** 3575-3583, 1981

23. Tomitani T and Tanaka E: Image reconstruction and noise evaluation in photon time-of-flight assisted positron emission tomography. *IEEE Trans Nucl Sci* **NS-28:** 4582-4589, 1981

24. Mullani NA, Ficke DC, Hartz R, et al: System design of fast PET scanners utilizing time-of-flight. *IEEE Trans Nucl Sci* **NS-28:** 104-107, 1981

25. Ter-Pogossian MM, Mullani NA, Ficke DC, et al: Photon time-of-flight-assisted positron emission tomography. *J Comput Assist Tomogr* **5:** 227-239, 1981

26. Wong WH, Mullani NA, and Wardworth G: Characteristics of small barium fluoride (BaF_2) scintillator for high intrinsic resolution time-of-flight positron tomography. *IEEE Trans Nucl Sci* **NS-31:** 381-386, 1984

27. Mullani NA, Gaeta J, Yerian K, et al: Dynamic imaging with high resolution time-of-flight PET camera - TOFPET I. *IEEE Trans Nucl Sci* **NS-31:** 609-613, 1984

28. Soussaline F, Comar D, Allemand R, et al: New developments in positron emission tomography instrumentation using the time-of-flight information. In *The Metabolism of the Human Brain Studied with Positron Emission Tomography*, Greitz T and Ingvar D, eds, Raven Press, New York, 1985, pp 1-12

29. Snyder DL: Some noise comparisons of data-collection arrays for emission tomography-systems having time-of-flight measurements. *IEEE Trans Nucl Sci* **NS-29:** 1029-1033, 1982

30. Politee DG, Holmes TJ, and Snyder DL: Effects of quantization of time-of-flight (TOF) measurements on image signal-to-noise ratio in TOF emission tomography. *IEEE Trans Nucl Sci* **NS-30:** 720-722, 1983

31. Huang SC, Hoffman EJ, Phelps ME, and Kuhl DE: Quantitation in positron emission computed tomography: 2. Effects of inaccurate attenuation correction. *J Comput Assist Tomogr* **3:** 804-814, 1979

32. Hoffman EJ, van der Stee LMAM and Ricci AR: Evaluation of the accuracy of the measured attenuation correction in positron tomography. *J Nucl Med* **24:** P10-P11 (Abstract) 1983

33. Hoffman EJ, Phelps ME, Huang SC, Plummer D, and Kuhl DE: Evaluating the performance of multiplane positron tomographs designed for brain imaging. *IEEE Trans Nucl Sci* **NS-29:** 469-473, 1982

34. Hoffman EJ, Huang SC, and Phelps ME: Quantitation in positron emission tomography: 1. Effect of object size. *J Comput Assist Tomogr* **3:** 299-308, 1979

35. Burnham CA, Alpert NM, Hoop B, Jr., et al: Correction of positron scintigrams for degradation due to random coincidences. *J Nucl Med* **18:** 604 (Abstract), 1977

36. Hoffman EJ, Phelps ME, Huang SC, et al: Effect of accidental coincidences in positron emission computed tomography. *J Nucl Med* **20:** 634-635 (Abstract), 1979

37. Derenzo SE: Method for optimizing side shielding in positron emission tomographs and for comparing detector materials. *J Nucl Med* **21:** 971-977, 1980

38. Holmes TJ, Ficke DC, and Snyder DL: Modeling of accidental coincidences in both conventional and time-of-flight positron-emission tomography. *IEEE Trans Nucl Sci* **NS-31:** 627-631, 1984

39. King PH: Noise identification and removal in positron imaging systems. *IEEE Trans Nucl Sci* **NS-28:** 148-151, 1981

40. Bergström M, Eriksson L, Bohm C, Blomqvist G and Litton J: Correction for scattered radiation in a ring detector positron camera by integral transformation of the projections. *J Comput Assist Tomogr* **7**: 42-50, 1982

41. Bruno MF, Huesman RH, Derenzo SE, and Budinger TF: Characterization of Compton Scattering in Emission Tomography. *J Nucl Med* **25**: P14, 1984

42. Wong WH and Adler S: Characterization of the scattered radiation fraction in PET or SPECT cameras with a novel phantom design. *IEEE Trans Nucl Sci* **NS-32**: 831-834, 1985

43. Holmes TJ: Predicting count loss in modern positron-emission tomography systems. *IEEE Trans Nucl Sci* **NS-30**: 723-727, 1983

44. Mazoyer BM, Roos MS, and Huesman RH: Dead time correction and counting statistics for positron tomography. *Phys Med Biol* **30**: 385-399, 1985

45. Derenzo SE: Initial characterization of a BGO-silicon photodiode detector for high resolution PET. *IEEE Trans Nucl Sci* **NS-31**: 620-626, 1984

46. Holmes TJ and Ficke DC: Analysis of positron-emission tomography scintillation-detectors with wedge faces and inter-crystal septa. *IEEE Trans Nucl Sci* **NS-32**: 826-830, 1985

47. Kesselberg M, Bohm C, Litton JE, et al: Design considerations of small crystal positron camera systems. *IEEE Trans Nucl Sci* **NS-32**: 907-911, 1985

48. Bohm C, Eriksson L, Bergström M, et al: A computer assisted ring detector positron camera system for reconstruction tomography of the brain. *IEEE Trans Nucl Sci* **NS-25**: 624-637, 1978

49. Brooks RA, Sank VJ, Talbert AJ, et al: Sampling requirements and detector motion for positron emission tomography. *IEEE Trans Nucl Sci* **NS-26**: 2760-2763, 1979

50. Herman GT: The mathematics of wobbling a ring of positron annihilation detectors. *IEEE Trans Nucl Sci* **NS-26**: 2756-2759, 1979

51. Herman GT: Data collection for cross-sectional image reconstruction by a moving ring of positron annihilation detectors. *J Comput Assist Tomogr* **3**: 261-266, 1979

52. Huang SC, Hoffman EJ, Phelps ME, et al: Sampling requirements of emission computed tomographic (ECT) scanners. *J Nucl Med* **20**: 609 (Abstract), 1979

53. Colsher JG and Muehllehner G: Effects of wobbling motion on image quality in positron tomography. *IEEE Trans Nucl Sci* **NS-28**: 90-93, 1981

54. Tanaka E, Nohara N, Yamamoto M, et al: "Positology" - the search for suitable detector arrangements for a positron ECT with continuous rotation. *IEEE Trans Nucl Sci* **NS-26:** 2728-2731, 1979

55. Takami K, Ishimatsu K, Hayashi T, et al: Design considerations for a continuously rotating positron computed tomograph. *IEEE Trans Nucl Sci* **NS-29:** 534-538, 1982

56. Cho ZH, Hong KS, Ra JB, et al: A new sampling scheme for the ring positron camera- dichotomic ring sampling. *IEEE Trans Nucl Sci* **NS-28:** 94-98, 1981

57. Huesman RH, Derenzo SE and Budinger TF: A two-position sampling scheme for positron emission tomography. In *Nuclear Medicine and Biology*, Raynaud C, ed., Pergammon Press, New York, Vol I, pp 542-545, 1983.

58. Derenzo SE, Budinger TF, and Vuletich T: High resolution positron emission tomography using narrow bismuth germanate crystals and individual photosensors. *IEEE Trans Nucl Sci* **NS-30:** 665-670, 1983

59. Derenzo SE, Budinger TF, Cahoon JL, Greenberg WL, Huesman RH, and Vuletich T: The Donner 280-crystal high resolution positron tomograph. *IEEE Trans Nucl Sci* **NS-26:** 2790-2793, 1979

60. Derenzo SE, Budinger TF, Huesman, RH, Cahoon JL and Vuletich T: Imaging properties of a positron tomograph with 280 BGO crystals. *IEEE Trans Nucl Sci* **NS-28:** 81-89, 1981

61. Eriksson L, Bohm C, Kesselberg M, et al: A four ring positron camera system for emission tomography of the brain. *IEEE Trans Nucl Sci* **NS-29:** 539-543, 1982

62. Schmitt D, Lecomte R, and LeBel E: Wedge-shaped scintillation crystals for positron emission tomography. *J Nucl Med* **27:** 99-104, 1986

63. Derenzo SE, Huesman RH, Budinger TF, Cahoon JL, and Vuletich T: High resolution positron emission tomography using 3 mm wide bismuth germanate crystals. *J Nucl Med* **25:** P46, 1984 (Reviewed Abstract)

64. Tomitani T, Nohara N, Morayama H, et al: Development of a high resolution positron CT for animal studies. *IEEE Trans Nucl Sci* **NS-32:** 822-825, 1985

65. Nohara N, Tanaka E, and Tomitani T: Analytical study of performance of high resolution positron emission computed tomographs for animal study. *IEEE Trans Nucl Sci* **NS-32:** 818-821, 1985

66. Computer Technology and Imaging, Inc. Knoxville, Tennessee, MODEL PT 931 ECAT Scanner System Description.

67. Hoffman EJ, Ricci AR, van der Stee LMAM, and Phelps ME: ECAT III- Basic design considerations. *IEEE Trans Nucl Sci* **NS-30:** 729-733, 1983

68. Hoffman EJ, Phelps ME, Huang SC, et al: Dynamic, gated and high resolution imaging with the ECAT III. *IEEE Trans Nucl Sci* **NS-33:** 452-455, 1986

69. Burnham CA and Brownell GL: A multi-crystal positron camera. *IEEE Trans Nucl Sci* **NS-19(3):** 201-205, 1972

70. Burnham C, Bradshaw J, Kaufman D, et al: One dimensional scintillation cameras for positron ECT ring detectors. *IEEE Trans Nucl Sci* **NS-28:** 109-113, 1981

71. Burnham CA, Bradshaw J, Kaufman D, et al: A stationary positron emission ring tomograph using BGO detector and analog readout. *IEEE Trans Nucl Sci* **NS-31:** 632-636, 1984

72. Burnham CA, Bradshaw J, Kaufman D, et al: Design of cylindrical shaped scintillation camera for positron tomographs. *IEEE Trans Nucl Sci* **NS-32:** 889-893, 1985

73. Stearns CW, Chesler DA, Kirsch JE, et al: Quantitative imaging with the MGH analog ring positron tomograph. *IEEE Trans Nucl Sci* **NS-32:** 898-901, 1985

74. Brownell GL, Burnham CA and Chesler DA: High resolution tomograph using analog coding. In *The Metabolism of the Human Brain Studied with Positron Emission Tomography*, Greitz T and D. Ingvar, eds, Raven Press, New York, 1985, pp 13-20

75. Ricci A, Hoffman E, Phelps M, et al: Investigation of a technique for providing a pseudo-continuous detector ring for positron tomography. *IEEE Trans Nucl Sci* **NS-29:** 452-456, 1982

76. Roney JM, Thompson CJ: Detector identification with 4 BGO crystals on a dual PMT. *IEEE Trans Nucl Sci* **NS-31:** 1022-1027, 1984

77. Eriksson L, Bergström M, Bohm Chr., et al: Figures of merit for different detector configurations utilized in high resolution positron cameras. *IEEE Trans Nucl Sci* **NS-33:** 446-451, 1986

78. Casey ME and Nutt R: A multicrystal two dimensional BGO detector system for positron emission tomography. *IEEE Trans Nucl Sci* **NS-33:** 460-463, 1986

79. Anger HO: Survey of radioisotope cameras. *ISA Trans* **5:** 311-334, 1966

80. Muehllehner G, Colsher JG, and Lewitt RM: A hexagonal bar positron camera: problems and solutions. *IEEE Trans Nucl Sci* **NS-30:** 652-660, 1983

81. Karp JS and Muehllehner G: Performance of a position-sensitive scintillation detector. *Phys Med Biol* **30:** 643-655, 1985

82. Muehllehner G and Karp JS: A positron camera using position-sensitive detectors: PENN–PET. *J Nucl Med* **27:** 90-98, 1986

83. Karp JS, Muehllehner G, Beerbohm D, et al: Event localization in a continuous scintillation detector using digital processing. *IEEE Trans Nucl Sci* **NS-33:** 550-555, 1986

84. Del Guerra A, Perez-Mendez V, Schwartz G, et al: Design considerations for a high spatial resolution positron camera with dense drift space MWPC's. *IEEE Trans Nucl Sci* **NS-30:** 646-651, 1983

85. Jeavons A, Hood K, Herlin G, et al: The high-density avalanche chamber for positron emission tomography. *IEEE Trans Nucl Sci* **NS-30:** 640-645, 1983

86. Lanza RC, Osborne LS, Holman BL, and Zimmerman RE: Mesh chambers for positron emission tomography. *IEEE Trans Nucl Sci* **NS-33:** 482-485, 1986

87. Anderson DF: Development of proportional counters using photosensitive gases and liquids. *IEEE Trans Nucl Sci* **NS-32:** 495-503, 1985

88. Woody CL, Petridou CI, and Smith CG: Properties of a barium fluoride-TMAE-multiwire proportional chamber detector for a large single crystal. *IEEE Trans Nucl Sci* **NS-33:** 136-139, 1986

89. Moszyński M, Vacher J, and Odru R: Application of the HR400 microchannel plate photomultiplier to study the light pulse shape from fast and slow scintillators by means of the single photon method. *Nucl Instr Meth* **204:** 141, 1982

90. Nieschmidt EB, Lawrence RS, Gentillon CD, et al: Count rate performance of a microchannel plate photomultiplier. *IEEE Trans Nucl Sci* **NS-29:** 196-199, 1982

91. Timothy JG: Electronic readout systems for microchannel plates. *IEEE Trans Nucl Sci* **NS-32:** 427-432, 1985

92. Senda M, Tamaki N, Yonekura Y, et al: Performance characteristics of Positologica III: a whole-body positron emission tomograph. *J Comput Assist Tomogr* **9:** 940-946, 1986

93. Yamashita Y, Uchida H, Yamashita T and Hayashi T: Recent development in detectors for high spatial resolution positron CT. *IEEE Trans Nucl Sci* **NS-31:** 424- 428, 1984

94. Uchida H, Yamashita T, Iida M, et al: Design of a mosaic BGO detector system for positron CT. *IEEE Trans Nucl Sci* **NS-33:** 464-467, 1986

95. Kume H, Muramatsu S, and Iida M: Position sensitive photomultiplier tubes for scintillation imaging. *IEEE Trans Nucl Sci* **NS-33:** 359-363, 1986

96. Capasso F: Avalanche photo diodes with enhanced ionization rates ratio: towards a solid state photomultiplier. *IEEE Trans Nucl Sci* **NS-30:** 424-428, 1983

97. Entine E, Reiff G, Squillante M, et al: Scintillation detectors using large area silicon avalanche photodiodes. *IEEE Trans Nucl Sci* **NS-30:** 431-435, 1983

98. Lecomte R, Schmitt D, Lightstone AW, et al: Performance characteristics of BGO-silicon avalanche photodetectors for PET. *IEEE Trans Nucl Sci* **NS-32:** 482-486, 1985

99. Petrillo GA, McIntyre RJ, Lecomte R, et al: Scintillation detector with large-area reach-through avalanche photodiodes. *IEEE Trans Nucl Sci* **NS-31:** 417-423, 1984

100. Squillante MR, Reiff G, and Entine G: Recent advances in large area avalanche photodiodes. *IEEE Trans Nucl Sci* **NS-32:** 563-566, 1985

101. Lightstone AW, McIntyre RJ, Lecomte R, et al: A bismuth germanate-avalanche photodiode module designed for use in high resolution positron emission tomography. *IEEE Trans Nucl Sci* **NS-33:** 456-459, 1986

102. McIntyre JA, Spross RL, and Wang KH: Construction of a positron emission tomograph with 2.4 mm detectors. *IEEE Trans Nucl Sci* **NS-33:** 425-427, 1986

103. Barton JB, Hoffman EJ, Iwanczyk JS, et al: A high-resolution detection system for positron tomography. *IEEE Trans Nucl Sci* **NS-30:** 671-675, 1983

104. Groom DE: Silicon photodiode detection of bismuth germanate scintillation light, *Nucl Instr Meth,* **219:** 141-148, 1984

105. Iwanczyk JS, Barton JB, Dabrowski AJ, et al: A novel radiation detector consisting of an HgI_2 photodetector coupled to a scintillator. *IEEE Trans Nucl Sci* **NS-30:** 363-367, 1983

106. Dahlbom M, Mandelkern MA, Hoffman EJ, et al: Hybrid mercuric iodide (HgI_2) – gadolinium orthosilicate (GSO) detector for PET. *IEEE Trans Nucl Sci* **NS-32:** 533-537, 1985

107. Derenzo SE, Budinger TF, Huesman RH, and Cahoon JL: Dynamic positron emission tomography in man using small bismuth germanate crystals. In *Positron Annihilation,* Coleman PG, Sharma SC, and Diana LM, eds. pp 935-945, North-Holland, New York, 1982.

108. Derenzo SE: Gamma-ray spectroscopy using small, cooled bismuth germanate scintillators and silicon photodiodes. *Nucl Instr Meth* **219:** 117-122, 1984

109. Derenzo SE, Budinger TF, and Huesman RH: Detectors for high resolution dynamic PET. In *The Metabolism of the Human Brain Studied with Positron Emission Tomography*, T. Greitz and D. Ingvar, Eds, Raven Press, New York, pp 21-31, 1985

110. N. Mullani, (1982), private communication.

111. Eriksson L, Bohm C, Kesselberg M, et al: A high resolution positron camera. In *The Metabolism of the Human Brain Studied with Positron Emission Tomography*, Greitz T and Ingvar D, eds, Raven Press, New York, 1985, pp 33-46

112. Wong WH: Designing a stratified detection system for PET cameras. *IEEE Trans Nucl Sci* **NS-33:** 591-596, 1986

113. Iida H, Kanno I, Miura S, et al: A simulation study of a method to reduce positron annihilation spread distributions using a strong magnetic field in positron emission tomography. *IEEE Trans Nucl Sci* **NS-33:** 597-600, 1986

114. Farukhi MR and Swinehart CF: Barium fluoride as a gamma ray and charged particle detector. *IEEE Trans Nucl Sci* **NS-18(1):** 200-204, 1971

115. Weber MJ and Monchamp RR: Luminescence of $Bi_4Ge_3O_{12}$: spectral and decay properties. *J Appl Phys* **44:** 5495-5499, 1973

116. Laval M, Moszyński M, Allemand R, et al: Barium fluoride: inorganic scintillator for subnanosecond timing. *Nucl Instr Meth* **206:** 169-176, 1983

117. Takagi K, and Fukazawa T: Cerium activated Gd_2SiO_5 single crystal scintillator. *Appl Phys Lett* **42:** 43-45, 1983